Publication 3

Dlala, E., Arkkio, A., "Measurement and analysis of hysteresis torque in a high-speed induction machine", *Electric Power Applications, IET*, Vol. 1(5): 737-742, September 2007.

Measurement and analysis of hysteresis torque in a high-speed induction machine

E. Dlala and A. Arkkio

Abstract: Hysteresis torque is analysed in a high-speed induction machine where the rotor is solid and made of a semihard magnetic material. The hysteresis torque is investigated at first with no load and experimental and numerical methods are considered. The analysis of hysteresis torque is then extended to rated conditions. The numerical modelling is conducted with accurate Preisach hysteresis models coupled with the finite-element method. The hysteresis torque is found to be relatively significant and represents 8% of the rated torque of the studied machine.

1 Introduction

High-speed induction machines (HSIMs) are increasingly used in many industrial applications. Because of the mechanical advantages, the rotor in most HSIMs is solid and made of a semihard material whose magnetic hysteresis loss produces torque in much the same way that a resistive loss does. In other words, since the hysteresis loss of the rotor keeps the magnetomotive forces of the rotor and stator at different angles, a finite torque will be created in the rotor known as 'hysteresis torque'.

In the past, a great majority of the works that were aimed at analysing hysteresis torque were devoted to the design and improvement of hysteresis motors [1–3] with only a few papers dealing with the hysteresis torque in induction motors [4, 5]. Moreover, most of the studies found in the literature were conducted using analytical methods, which involved approximations to the rotor magnetic hysteresis properties using, for example, parallelograms or complex permeability. Such approximations may significantly affect the accuracy of the computed quantities. More recently, numerical methods, such as the finite-element method (FEM), have come to the force as tools for modelling electromagnetic devices, and the problem of modelling hysteresis phenomena has been widely considered in the literature [6, 7]. In the work of Adly [2], the Preisach model was integrated into a digital simulation for investigating a three-phase hysteresis motor. In the work of Hong *et al.* [3], a vector hysteresis model was combined with a FEM analysis in order to compute the hysteresis torque by calculating the area of the hysteresis loop.

The rotor of the HSIM consists of a solid iron core encircled with a thin copper layer which is short-circuited at the end-rings. The rotor is made of a semihard solid material in order to endure the centrifugal forces resulting from the high surface speed ($\sim$200 m/s). The semihard magnetic material exhibits relatively large hysteresis loops and hence, substantial hysteresis torque. Only at no load can hysteresis torque be segregated from the measured total torque. Unfortunately, such a measurement cannot be relied upon to analyse hysteresis torque at a rated load because loading completely changes the flux distribution of a solid rotor, and the hysteresis torque changes accordingly (see Fig. 1). On the one hand, a designer or user of an electrical machine is mainly interested in estimating hysteresis torque at loading conditions; on the other hand, achieving this by measurement is virtually impossible. Only simulation techniques have a feasibe capability for analysis. Therefore, our strategy of analysis is to build-up a rigorous simulation technique validated by the measured no-load hysteresis torque, and after such a validation, we can use and rely on the simulation technique to analyse and predict hysteresis torque for a loaded machine.

The numerical simulation technique is based on computing the magnetic field by a 2D-FEM taking hysteresis into account. The FEM model is rather simplified where only the rotor is considered. It is our intention to incorporate the inverted Preisach model [8] into the FEM analysis where the fixed-point technique will be the interface between the hysteresis engine and the FEM solution.

2 Method of measurement

The hysteresis torque changes sign at the synchronous speed (no load) and causes a jump in the input power of the machine. The only torque or loss component that changes significantly and abruptly when passing the synchronous speed is assumed to correspond to the hysteresis torque. Near the synchronous speed, the torque components associated with the harmonics and friction are approximately constant (see Fig. 2). The jump of power, which is associated with the hysteresis torque, is determined by operating the machine at small slips in motoring and generating modes and then extrapolating to the synchronous speed.

The HSIM specifications are given in Table 1. The experimental set-up (Fig. 3) proposed to measure the hysteresis torque consisted mainly of a control circuit and the HSIM, which was mechanically coupled to a slip-ring induction machine. The critical task in this measurement was the frequency control of the current supplied to the slip-ring rotor so that the desired small slips were precisely achieved. The input power of the HSIM was measured along one revolution made by the rotor relative to the synchronous speed.

doi:10.1049/iet-epa:20060472

Paper first received 21st November 2006 and in revised form 12th March 2007

The authors are with the Laboratory of Electromechanics, Helsinki University of Technology, PO Box 3000, FI-02015 TKK, Finland

E-mail: emad.dlala@ttk.fi

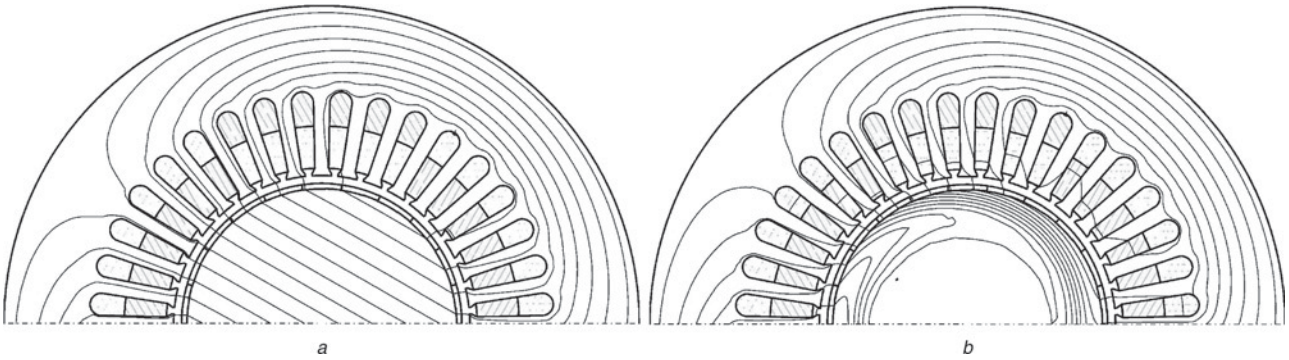

Fig. 1 *Flux distribution in the high-speed induction machine*
a At no load (slip = 0.0%)
b At a loading condition (slip = +0.01%)

The power versus rotor angle was recorded by the measuring system for each slip. The average power was then taken for one complete revolution in order to obtain the power versus slip graph. Fig. 4 shows a particular example of the power versus slip curve when the line current was 100 A. The square points represent the average values of the power taken from the HSIM. The points were connected by cubic spline interpolation and then extrapolated to the synchronous speed. The difference of power ΔP is indicated by the double-arrowed line in Fig. 4, and the correspondent hysteresis torque can be computed according to

$$T_h = \frac{\Delta P}{2\omega_e} \text{ (N m)} \tag{1}$$

where ω_e is the electrical angular frequency of the supply frequency. The hysteresis torque value corresponding to the case of Fig. 4, where the line current was 100 A, is 1.27 N m. Similar measurements were carried out by varying the input voltage for currents ranging from 25 up to 195 A whose hysteresis torque values are shown in Fig. 5. The no-load current at rated voltage and rated frequency is 140 A corresponding to 2.75 N m of hysteresis torque.

3 Numerical modelling

The HSIM is considered to be a quasistatic magnetic system. The magnetic field of the machine is assumed to be two-dimensional and only the rotor cross-section is used for the computation of the hysteresis torque. The end-ring effects are neglected in the computation. Their influence on the accuracy of the hysteresis torque at no load is negligible, but they might be more important at loaded conditions. Such an investigation will be pursued by the authors in future work.

The analysis of the hysteresis torque is based on the computation of the magnetic flux densities in the elements of the mesh and then using a Maxwell stress tensor to compute the torque. In the FEM analysis, a rotating field subjected to the rotor is created by imposing a sinusoidal flux on the outer surface of the airgap. This flux then rotates around the rotor periphery at a constant speed and only the fundamental wave of the flux is considered. The higher harmonics in the airgap caused by the stator slots are difficult to penetrate the copper layer of the rotor into the solid iron. However, the lower-order harmonics caused by saturation might force the airgap flux to be nonsinusoidal, and this problem might require an iterative procedure if the boundary condition was forced to be nonsinusoidal. On the other hand, a more comprehensive model that engages both the rotor and stator in the computation would automatically solve the problem. Such a model is the aim of future research.

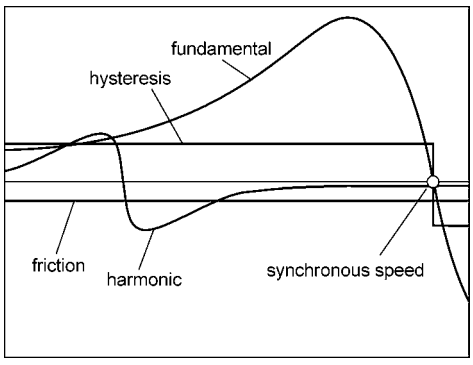

Fig. 2 *Representation of the torque components (fundamental, harmonic, friction, and hysteresis) produced by an induction machine*

3.1 Magnetic field formulation

The interface between the inverted Preisach model and the FEM solution is established by the fixed-point iterative procedure. This nonlinear technique handles the constitutive relationship between the magnetic field intensity $\boldsymbol{H}$ and the flux density $\boldsymbol{B}$, and can be written in the following manner

$$\boldsymbol{H} = \nu\boldsymbol{B} + \boldsymbol{R} \tag{2}$$

Table 1: Main parameters of the high-speed induction machine

Parameter	Value
Number of poles	2
Number of phases	3
Number of stator slots	36
Outer diameter of stator core (mm)	290
Diameter of solid iron in the rotor (mm)	123
Rated voltage (V)	400
Rated power (kW)	200
Rated torque (N m)	63
Rated frequency (Hz)	500
Connection	Delta

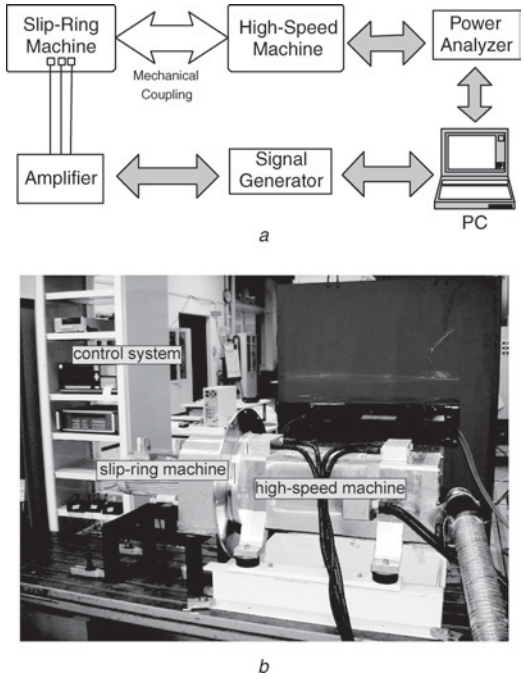

Fig. 3 *Experimental setup for measuring hysterisis torque in the high-speed induction machine*

a Sketch of the setup layout
b Photograph of the setup layout

where ν is a properly chosen constant, and $\boldsymbol{R}$ is a residual nonlinearity, which is to be determined iteratively.

At no load, all conductivities of the copper and iron are set to zero. Appropriate Maxwell's equations and the constitutive law (2) are formulated as

$$\nabla \times \mathcal{F}(\nabla \times A) = 0 \tag{3}$$

in which A is the z-component of the vector potential $\boldsymbol{A}$ in the x-y plane perpendicular to the shaft. If ν_0 is the reluctivity of the air, the function $\mathcal{F}$, which describes the regions from the magnetic material point of view, can be defined as

$$\mathcal{F}(B) = \begin{cases} \nu_0 B & \Rightarrow \text{ linear regions} \\ \mathcal{H}(B) & \Rightarrow \text{ nonlinear hysteretic regions} \\ \nu(|B|) & \Rightarrow \text{ nonlinear single-valued regions} \end{cases} \tag{4}$$

At rated conditions, since the rotor is solid, eddy currents are dominant and responsible for changing the flux

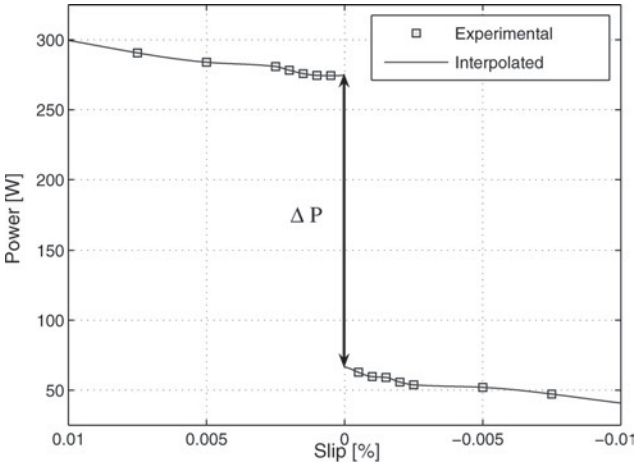

Fig. 4 *Average powers measured as a function of of the slip*

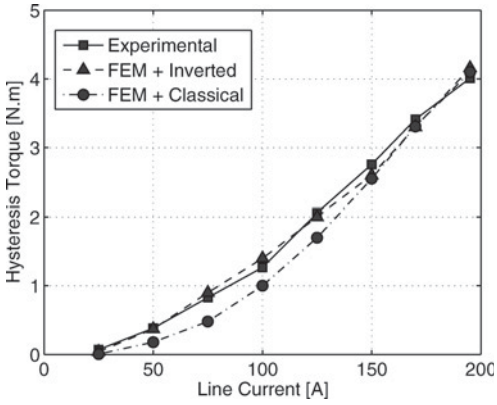

Fig. 5 *Experimental hysteresis torque values compared with the computed ones by the FEM analysis integrated with the inverted Preisach model and the classical Preisach model*

distribution in the solid iron (see Fig. 1). Thus, (3) is no more valid and should be replaced by

$$\nabla \times \mathcal{F}(\nabla \times A) + \sigma \frac{\partial A}{\partial t} = 0 \tag{5}$$

where σ is the electrical conductivity of the solid iron and t is time. Since we are interested only in the torque developed by hysteresis, the conductivity of the copper layer is set to zero.

Actually, the solution of (5) gives the torque produced by both hysteresis and the resistive loss of the iron. Although the magnetic field solutions of the single-valued and hysteretic cases would be slightly different, the resistive torque can only be segregated by applying the single-valued characteristic in (5) in which hysteresis is not considered.

In order to ensure rotating sinusoidal flux on the outer surface of the rotor, the magnetic vector potential must satisfy the following boundary condition

$$A_b(\phi, t) = \hat{A}_b \sin(p\phi - w_r t) \tag{6}$$

where ϕ is the angle of the particular point on the boundary, ω_r is the angular slip-frequency of the rotor, $\hat{A}_b$ is the peak value of A_b, and p is the number of pole pairs of the motor. The amplitude of the vector potential on the boundary $\hat{A}_b$ is computed from

$$\hat{A}_b = \frac{r}{p}\hat{B} \tag{7}$$

where $\hat{B}$ is the peak flux density of the fundamental component in the airgap, and r is the radius of the boundary circle.

3.2 Hysteresis torque computation

The electromagnetic torque is computed through Maxwell stress tensor from a surface integral as

$$T_e = \oint_S r \times \left\{ \frac{1}{\mu_0}(\boldsymbol{B} \cdot \boldsymbol{n})B - \frac{1}{2\mu_0}B^2 \boldsymbol{n} \right\} \mathrm{d}S \tag{8}$$

in which μ_0 is the permeability of free space and $\boldsymbol{n}$ is the unit normal vector of the integration surface S. Using polar coordinates, (8) can be transformed to a line integral. As described by Arkkio [9], the line integral can be replaced by a surface integral over the airgap with circle of radius r

$$T_e = \frac{l_{ef}}{\mu_0(r_{\text{out}} - r_{\text{in}})} \int_{S_{\text{ag}}} r B_r B_\varphi \, \mathrm{d}S \tag{9}$$

where l_{ef} is the effective core length of the motor, and B_r and B_φ stand for the radial and tangential components of the flux density. r_{out} and r_{in} are the outer and inner radii of the airgap, and S_{ag} represents the cross-section area of the airgap.

4 Hysteresis model

The inclusion of magnetic hysteresis within electromagnetic field equations is indispensable for our analysis and, thus, has to be given special treatment. The relationship $\mathcal{H}(B)$ in (4) needs a vector hysteresis model that can correctly describe the nonlinear hysteretic behaviour. We shall apply the inverted Preisach model developed as detailed in [8]. In FEM formulations, employing the magnetic vector potential $\boldsymbol{A}$ as the unknown, the magnetic flux density $\boldsymbol{B}$ is directly obtained as the output quantity [10]. Most of the well-known hysteresis models, such as the Preisach model and the Jiles model [11, 12], are standardly H-based. Thus, they are not suitable for modelling hysteresis when coupled with the $\boldsymbol{B}$-oriented FEM equations because the models have to be iteratively inverted in order to be suited for the problem.

The main advantage of the inverted Preisach model over other Preisach-type models [6, 7] relates to its fastness when used for FEM problems formulated by the vector potential since the model computes the magnetic field H directly. In addition, the inverted Preisach model is more accurate because it is suitable to cope with the congruency problem.

In the inverted Preisach model, all curves starting from the reversal points with the same flux density B have the same shape. Therefore, in contrast to the classical Preisach model, which is based on the vertical congruency, the inverted Preisach model is based on the horizontal congruency and thus not influenced by the relative sharp change of magnetisation near the coercive field.

The classical Preisach model works to interpolate the modelled branches from the Everett function where all curves starting from the reversal points with the same field H have the same shape. In most magnetic materials, due to the relative large change of the magnetization (dB/dH) near the coercive field, most of the reversal points are strongly localised near the coercive field. Therefore, only the larger loops that are close to saturation could be improved by the use of first-order reversal curves, and for the minor loops that shrink inside the major loop, the congruency problem would then appear as a major drawback.

On the other hand, in the inverted Preisach model, the interpolation is controlled by the axis of the flux density B; the projection on the B axis specifies which pattern should correspond to the modelled curve. Therefore, the inverted Preisach model is not influenced by the sharp change of the magnetisation near the coercive field. The reversal points are lying on the descending (or ascending) branch of the major loop. Even though the same first-order reversal curves are used to identify the classical Preisach model and the inverted Preisach model, the 'reversal points' are relatively uniformly distributed with respect to the magnetic flux B while sharply jumping with respect to the magnetic field H.

The scalar quantity H of the inverted Preisach model is computed according to the following numerical formula

$$H = -F(-B_0^+, B_0^-) + 2\sum_{k=1}^{n} F(B_k^+, B_{k-1}^-) - F(B_k^+, B_k^-) \tag{10}$$

where $F(B_k^+, B_k^-)$ is the inverted Everett function corresponding to the specific reversal points $k = 1, 2, \ldots, n$ of the scalar magnetic flux density B, and $F(-B_0^+, B_0^-)$ is the inverted Everett weight of the demagnetising state. The superscripts $(+, -)$ refer to the increasing and decreasing values of the input B, respectively.

To account for rotating fields, such as the ones revolving in electric rotating machines, the extension of the scalar model to a vector model is needed. The magnetic field vector $\boldsymbol{H}$ can be expressed in two-dimensions as

$$\boldsymbol{H} = \int_{-\pi/2}^{\pi/2} \mathbf{e}_\theta B\{B_\theta\}\, d\theta \cong \sum_{i=1}^{N} \mathbf{e}_{\theta_i} B\{B_{\theta_i}\} \tag{11}$$

in which $H_\theta = B\{B_\theta\}$ is the scalar magnetic field in the direction $\mathbf{e}_\theta$, and $B_\theta = |\boldsymbol{B}| \cos(\vartheta_B - \theta)$ is the projected magnetic flux with the direction of the magnetic flux vector $\boldsymbol{B}$, specified by ϑ_B. In numerical computations, it is useful to discretise the interval $\theta \in [-\pi/2, \pi/2]$ as $\theta_i = -\pi/2 + (i-1)\pi/N$, where $i = 1, \ldots, N$ and N is the number of directions, that is, the magnetic field vector is the vectorial sum of the scalar magnetic fields yielded by the individual scalar hysteresis models.

5 Results and discussion

In this section, the numerical results obtained by implementing the procedures of sections 3 and 4 will be shown and discussed. First, the simulation model is validated by the experimental results obtained at no load. For the sake of comparison, in addition to the inverted Preisach model, the classical Preisach model is applied in the FEM analysis likewise. The hysteresis models are identified using first-order reversal curves. The total number of the finite elements in the simulated geometry was 2023; 906 of which were nonlinear and the rest were linear. The inverted Preisach vector model and the classical Preisach vector model consistently composed of six directions in the computations. The online inversion of the classical Preisach model was optimally realised by a combined bisection-modified Regula–Falsi (BMRF) iterative search [13].

The time-stepping solution of the magnetic field behaviour was run over some periods of the boundary condition until reaching the steady-state. Since a slotless geometry (solid rotor) was considered, the time variation of the torque was expected to be constant. As an example, using two electrical periods (slip–0.001%) starting from the zero field as an initial state, the computed instantaneous electromagnetic torque for the amplitude of the fundamental flux component corresponding to 100 A using the inverted Preisach vector model is shown in Fig. 6. Clearly, having only three directions in the vector model caused a relatively sinusoidal alternation of the torque while having six directions gave a more flat variation as was expected.

Similar computations were carried out for other operational points ranging from 25 up to 195 A. The hysteresis torque was computed and compared with the measured results as presented in Fig. 5; the computed values of the hysteresis torque correspond to the average values of the steady-state torque. This comparison shows that at higher currents the FEM results based on the inverted vector model and on the classical vector model have given similar good agreements. At lower currents, however, the FEM results based on the classical vector model started deviating from the trend of the measured results, while the FEM results based on the inverted vector model were still maintaining almost the same manner of accuracy.

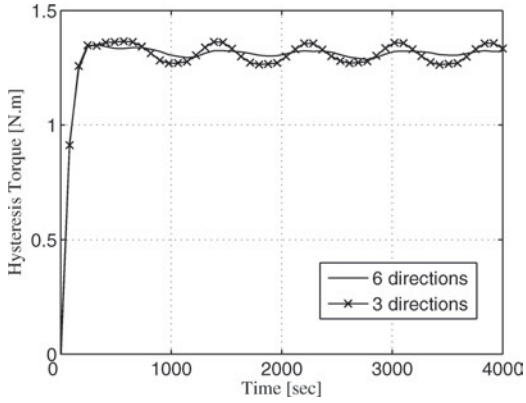

Fig. 6 *Instantaneous hysteresis torque computed by the inverted Preisach vector model incorporated into FEM model at slip 0.001%*

The first reason behind the deviation is the inaccuracy of the classical Preisach model for estimating the minor loops as shown in Fig. 7. The second reason can be associated with the accumulation of the error calculations resulted from using the BMRF method in inverting the classical Preisach vector model.

Computational efficiency was a natural consequence of the inverted Preisach model since the model gives $\boldsymbol{H}$ directly from $\boldsymbol{B}$. It was found that the overall computation time was 10 times shorter than that when incorporating the classical Preisach model.

The simulation technique of the hysteresis torque using the inverted Preisach model proved accurate and fast, and thus can be reliably used to analyse hysteresis torque for a loaded machine. The hysteresis torque together with the iron-resistance torque were computed (Fig. 8) at varied slips. Then, the resistive torque was subtracted by considering only the single-valued curve where hysteresis was omitted; the remaining torque represents the hysteresis torque. At the rated slip (1.1%), the simulated hysteresis torque was 5.12 N m. This corresponds to 8% of the rated machine torque.

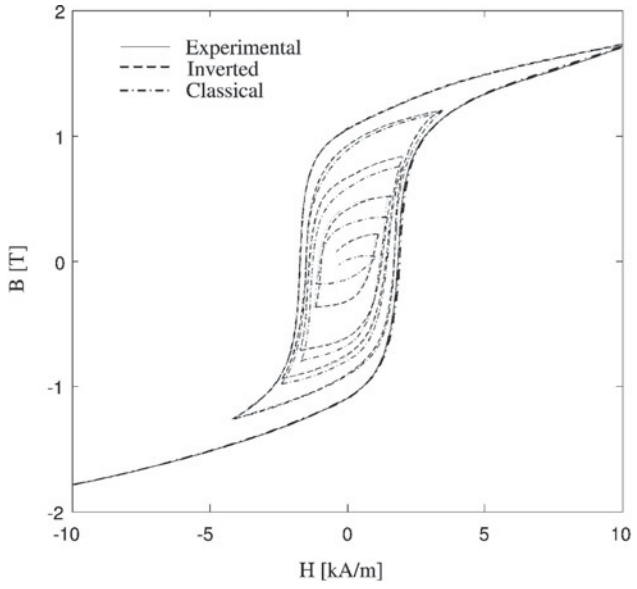

Fig. 7 *Hysteresis loops of semihard material predicted by inverted Preisach model, classical Preisach model, and compared with experimental data*

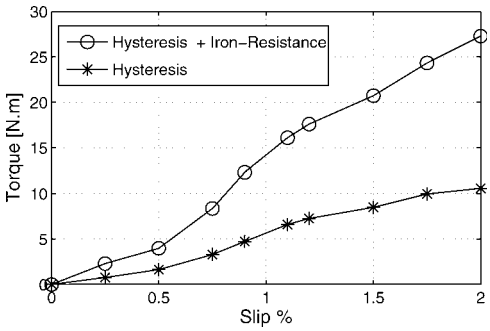

Fig. 8 *Simulations of the iron-resistance torque and the hysteresis torque at varied slips*

6 Conclusion

This paper dealt with analysing hysteresis torque in a high-speed induction machine. A numerical technique based on the finite-element method and the inverted Preisach model was proposed and validated with experimental data at no load. The numerical technique was then used to simulate hysteresis torque for loading conditions. The analysis revealed that the hysteresis torque represented 8.13% of the rated torque in the studied machine.

The main goal of this paper was to introduce a method that allows segregation of the hysteresis torque from the total torque produced in an induction machine by using a rather simple model. In this work, a few assumptions had to be made in assessing the hysteresis torque. These assumptions are insignificant at no-load conditions, but they can have a greater impact under loading conditions. In particular, the copper layer and the end-rings should be included in the analysis to evaluate their effects on the results. A more comprehensive model should also take the effects of slotting harmonics and iron saturation into account. Such an analysis in which most of these restricting assumptions are omitted is currently being conducted by the authors. Initial results suggest that our simple model presented in this work is adequate for use at no load, but may differ slightly with the comprehensive model at the rated load. However, this comprehensive model, which considers the rotor and stator together, requires much more computation time for each simulation. That is because simulating one period of the flux in the rotor requires running many periods of the stator supply depending on the slip, which was not the case in the rotor model. A comparison, in terms of accuracy and efficiency, of the two models using the same proposed method would seem to be fruitful and will be conducted in the near future.

7 Acknowledgment

The authors would like to thank the following organisations for their financial support: the Academy of Finland, the Finnish Cultural Foundation, and Fortum Corporation.

8 References

1 Zaher, F.A.A.: 'An analytical solution for the field of a hysteresis motor based on complex permeability', *IEEE Trans. Mag.*, 1990, **5**, (1), pp. 156–162
2 Adly, A.A.: 'Performance simulation of hysteresis motors using accurate rotor media models', *IEEE Trans. Mag.*, 1995, **31**, (6), pp. 3542–3544
3 Hong, S., Kim, H., Kim, H., and Jung, H.: 'Torque calculation of hysteresis motor using vector hysteresis model', *IEEE Trans. Mag.*, 2000, **36**, (4), pp. 1932–1935

4 Arkkio, A., Niemenmaa, A., and Saitz, J.: 'Hysteresis torque in a cage induction motor'. ICEM, Istanbul, September 1998, pp. 1494–1499
5 Wieser, R., and Lechner, A.: 'The influence of rotor hysteresis effects on space phaser models of induction machines'. ICEM, Vigo, vol. 1, pp. 119–124
6 Mayergoyz, D.: 'Mathematical models of hysteresis' (Springer-Verlag, New York, 1991)
7 Dlala, E., Saitz, J., and Arkkio, A.: 'Hysteresis modeling based on symmetric minor loops', *IEEE Trans. Magn.*, 2005, **41**, pp. 2343–2348
8 Dlala, E., Saitz, J., and Arkkio, A.: 'Inverted and forward Preisach models for numerical analysis of electromagnetic field problems', *IEEE Trans. Magn.*, 2006, **42**, (8), pp. 1963–1973
9 Arkkio, A.: 'Analysis of induction motors based on the numerical solution of the magnetic field and circuit equations'. Doctoral Thesis, Acta Polytechnica Scandinavica, no. 59, September 1987 http://lib.tkk.fi/Diss/198X/isbn951226076X/
10 Bottauscio, O., Chiarabaglio, D., Chiampi, M., and Repetto, M.: 'A hysteretic periodic magnetic field solution using Preisach model and fixed-point technique', *IEEE Trans. Magn.*, 2005, **31**, pp. 3548–3550
11 Sadowski, N., Batistela, N.J., Bastos, J.P.A., and Lajoie-Mazenc, M.: 'An inverse Jiles–Atherton model to take into account hysteresis in timestepping finite-element calculations', *IEEE Trans. Magn.*, 2002, **38**, (2), pp. 797–800
12 Takahashi, N., Miyabara, S., and Fujiwara, K.: 'Problems in practical finite element analysis using Preisach hysteresis model', *IEEE Trans. Magn.*, **35**, (3), pp. 1243–1246
13 Saitz, J.: 'Magnetic field analysis of electric machines taking ferromagnetic hysteresis into account'. Doctoral thesis, Acta Polytechnica Scandinavica, no. 107, 2001, p. 123, http://lib.tkk.fi/Diss/2001/isbn9512256908/